Journal of Pharmaceutical Sciences xxx (2018) 1-8

Contents lists available at ScienceDirect

Journal of Pharmaceutical Sciences

journal homepage: www.jpharmsci.org

Pharmaceutics, Drug Delivery and Pharmaceutical Technology

Modeling Glucose Transport From Systemic Circulation to Sweat

Terri D. La Count [1], Andrew Jajack [2], Jason Heikenfeld [2], Gerald B. Kasting [1, *]

[1] Division of Pharmaceutical Sciences, James L Winkle College of Pharmacy, University of Cincinnati, Cincinnati, Ohio 45267
[2] College of Engineering and Applied Sciences, University of Cincinnati, Cincinnati, Ohio 45221

ARTICLE INFO

Article history:
Received 6 July 2018
Revised 30 August 2018
Accepted 20 September 2018

Keywords:
biomarkers
glucose
mathematical model
sensor
sweat

ABSTRACT

Sweat sensing may provide a noninvasive means of estimating blood biomarker levels if a number of technological hurdles can be overcome. This report describes progress on a physiologically based transport model relating sweat glucose and key electrolyte concentrations to those in blood. Iontophoretically stimulated sweat glucose and fasted blood glucose were simultaneously measured in 2 healthy human subjects. Sweat glucose was measured with a novel, prototype skin sweat collection/analysis system and blood glucose with a commercial fingerstick glucometer. These data, in combination with data from 3 published studies, were used to calibrate a dynamic mathematical model for glucose transport and uptake in human skin, followed by extraction into sweat. Model simulations revealed that experimental and literature sweat glucose values were well represented under varying physiologic conditions. The glucose model, calibrated under a variety of experimental conditions including electrical enhancement, revealed a 10 min blood-to-sweat lag time and a sweat/blood glucose level ranging from 0.001 to 0.02, depending on the sweat rate. These values are consistent with those reported in the literature. The developed model satisfactorily described the sweat-to-blood relationship for glucose concentrations measured under different conditions in 4 human studies including the present pilot study. The algorithm may be used to facilitate sweat biosensor development.

Introduction

Diabetes in the United States affects approximately 10% of the general population. Diabetic complications of neuropathy, glaucoma, ketoacidosis, hypertension, stroke, kidney and heart diseases, and other medical costs exceeded $245 billion in 2012.[1] Diabetic risks can be reduced through tight glycemic control, most commonly assessed by finger pricking. Unfortunately, this manner of invasive glucose sampling reveals only glucose level snapshots, meaning fluctuations over time are likely not detected. This limitation has served as an impetus for continuous glucose monitoring (CGM) devices, which capture temporal blood glucose swings through frequent assessments, but still require confirmatory blood glucose measurements.[2]

An early CGM contender was the GlucoWatch,™[3] which delivered interstitial fluid (ISF) for glucose readings to the device on the skin surface by reverse iontophoresis.[4] Although it provided reliable physiologic correlations between steady-state glucose ISF levels[5] and blood, lack of widespread acceptance for GlucoWatch™ can be attributed to measurement inaccuracies (stemming from blood glucose/sensor reading lag times), requisite fingerstick calibrations, and skin irritation engendered by the delivery technique.[6] Current CGM devices,[7] some of which use a glucose sensor inserted dermally for frequent ISF glucose testing, still require twice-daily calibrations with finger blood glucose measurements and experience inaccuracy issues. Recently, multifaceted approaches have led to pivotal advances in biosensor research, piquing renewed interest in noninvasive biofluid monitoring,[8] with skin viewed as particularly promising.

Current noninvasive skin biosensor research is focused on sweat biomarker sampling.[9] Besides the ease and convenience of collection capability, sweat analysis is especially promising because biomarkers generally partition into sweat at levels that correlate to blood, making it a biomarker-rich sampling matrix.[9] Furthermore, sweat has a reduced potential for adulteration, and facile methods (e.g., iontophoresis) exist for increasing sample volumes, enabling

Conflicts of interest: J.H. is a co-founder of Eccrine Systems Inc., a company which is commercializing sweat sensing technologies. No competing financial interests exist for T.D.L.C., A.J., and G.D.K.

* *Correspondence to:* Gerald B. Kasting (Telephone: +1-513-558-1817).
E-mail address: Gerald.Kasting@uc.edu (G.B. Kasting).

https://doi.org/10.1016/j.xphs.2018.09.026
0022-3549/

Nomenclature

$C_{i\ DE}$	Concentration of biomarker i in dermis (mol/L)
$C_{i\ ISF}$	Concentration of biomarker i in interstitial fluid (mol/L)
$C_{i\ k}$	Biomarker i concentration in skin layer k (mol/L)
$C_{i\ m}$	Biomarker i concentration in sweat gland section m (mol/L)
$C_{i\ p}$	Concentration of biomarker i in plasma (mol/L)
$C_{i\ SG}$	Concentration of biomarker i in sweat gland (mol/L)
C_i (t)	Concentration as a function of time t (mol/L)
$C_{i\ VE}$	Concentration of biomarker i in viable epidermis
Cl_i, Na_i, K_i	Intercellular (luminal) chloride, sodium, and potassium concentration (mol/L)
Cl_s, Na_s, K_s	Serosal (extracellular) chloride, sodium, and potassium concentration (mol/L)
ΔC_i^{TM}	Transmembrane concentration difference of biomarker i (mOsm/L)
$D_{i\ ISF}$	Diffusivity of biomarker i in interstitial fluid (cm^2/s)
$D_{i\ k}$	Diffusivity of biomarker i in skin layer k (cm^2/s)
$D_{i\ m}$	Diffusivity of biomarker i in sweat gland section m (cm^2/s)
$D_{i\ SG}$	Diffusivity of biomarker i in sweat gland (cm^2/s)
F	Faraday's constant (C/mol)
J_{NaK}	Flux of NaK pump (mol/m^2)
J_{NKCC}	Flux of NKCC cotransporter (mol/m^2)
$J_{source\ i}$	Flux that serves as source of biomarker i (mol/s)
J_w^{TM}	Transmembrane water flux (m^3/s)
k_b	Backward reaction rate for NKCC cotransporter (1/s)
$k_{de\ i}$	Dermal clearance constant for biomarker i (1/s)
k_f	Forward reaction rate for NKCC cotransporter (1/s)
K_m	Michaelis-Menten analyte affinity constant (mol/L)
$K_{SG/ISF}$	Partition coefficient of biomarker i between sweat gland and interstitial fluid
$k_{uptake\ ik}$	Metabolic uptake rate for biomarker i in skin layer k (mol/m^3 s)
L_p^{TM}	Transmembrane hydraulic permeability of water ($\mu m/s$)
m	Sweat gland sections: acrosyringium, resorptive duct, secretory coil
P_i	Permeability coefficient of biomarker i (cm/s)
R	Gas constant (J/mol K)
S	Surface area of membrane (cm^2)
SA	Capillary surface area (cm^2)
T	Temperature (K)
t	Time (s)
u	Fluid velocity in sweat gland (m/s)
V_k	Volume of skin layer k (L)
V_{max}	Michaelis-Menten maximum uptake rate (mol/Ls)
V_p	Volume of plasma (L)
z	Longitudinal sweat gland/skin axis (cm)
z_i	Valence of biomarker i

Greek symbols

ψ	Potential difference across membrane (V)
ρ_{NaK}	Density of NaK pump (mol/cm^2)
ρ_{NKCC}	Density of NKCC cotransporter (mol/cm^2)
υ_{NaK}	Turnover rate of NaK pump
υ_{NKCC}	Turnover rate of NKCC cotransporter
υ_w	Partial molar volume of water (m^3/mol)

sampling under sedentary conditions as exemplified by infantile cystic fibrosis diagnoses.[10] Advantages for skin-intimate wearable biosensors that incorporate sweat as the biofluid sampling matrix include (1) improved time resolution for diagnostic detection/treatment, affording immediate health assessments and (2) elimination of sample transport problems encountered with free-standing biosensor platforms. Complementary to such development is the theoretical basis of the biophysical processes pertinent to biomarker transport.

A better understanding of the glucose skin/appendageal transport processes is imperative for facilitating the development of noninvasive glucose sensing devices. Although components of this relationship—detailed capillary transport,[11] cellular glucose transport,[12-15] and dynamic skin layer modeling[15-17]—exist in the literature, a complete mathematical model for predictive biomarker estimates for sweat gland (SG) delivery is lacking. Our objective was to develop a computational model, based on SG and skin physiology/biochemistry, which can provide a detailed mechanistic and chronological understanding of the various transport and biochemical processes impacting glucose delivery to sweat from systemic circulation. Accurate modeling of these dynamics can shed insight into the transport parameters that most impact glucose delivery, thereby facilitating noninvasive biosensor development. Ultimately, sweat glucose may not be competitive with existing CGM techniques; regardless, we explore sweat glucose in detail here because it is well studied and therefore useful in terms of comparing modeling and *in vivo* results. Such a model may potentially be applied to other biomarkers (metabolites, amino acids, proteins), further facilitating health diagnoses.

Experimental Sweat Measurements

Sweat glucose samples were obtained in an institutional review board–approved human subjects study described elsewhere.[18] Six healthy volunteers (5 male, 1 female) between the ages of 20 and 40 years participated in the study. These individuals fasted for 8 h before the start and throughout the entire duration of the experiment. All experiments began at ~9 AM. After attaching a custom-made testing device to the clean volar forearm skin at a distance of 15 cm from the distal wrist crease of each volunteer, sweat was initiated via iontophoretic delivery of carbachol.[19,20] Sample contamination was mitigated by using a thin layer of oil before device attachment. At 20 min after initial sweat stimulation (to ensure attainment of stable sweating), a 3-pronged experimental protocol was followed. First, the sweat rate was measured gravimetrically for 10 min, with blood glucose measured concurrently (at the midway point) using a fingerstick glucometer outfitted with Accu-Chek Aviva Plus test strips (Roche Diagnostics) rated within ±10%-15% accuracy. The finger to be tested was first cleaned with soap/water, then wiped with isopropyl alcohol, and finally rinsed with water and dried. Finally, sweat was collected for 45 min, and then extracted from the absorbent hydrophilic mesh collection disks (TX609 TechniCloth; Texwipe) by centrifugation and stored in a −20°C freezer. For sweat glucose determinations, sweat samples were first thawed to room temperature and diluted 2-fold with the buffer provided with the assay to mitigate pH effects on enzyme activity. They were then read via a microplate reader (Synergy H1; BioTek) with an enzymatic glucose assay (Amplex Red Glucose Assay; Thermo Fisher Scientific). Sweat rate and blood glucose measurements from before and after each collection period were

averaged to determine the average values during the collection period. The 3-step sequence was repeated 6-8 times per volunteer. The modeled data shown represents the results of 2 subjects.

Computational Modeling Method

Overview

Electrolyte and fluid transport is foundational to sweat generation, osmoticity, and pH. As these factors may also impact other biomarker transport, a modeling framework incorporating the basic physiology of the SG was initially developed for key electrolyte transport. Due to the flexibility of the model, this approach facilitated the extension of the model to other biomarkers, specifically glucose. Of particular interest in using this biomarker as an example was the correlation between glucose biomarker concentration and sweat rate.

Development of a biomarker transport model from the circulatory system to emergent sweat entails the driving forces of diffusion, and where applicable, convection, through the capillaries, ISF, and the 3 SG compartments. Additional pertinent factors for biomarker transport include electrostatic interactions, active transport mechanisms, interplay between sweat rate and final sweat composition, and applied electric fields.

Steady-state analytical solutions are the first step in modeling such processes,[9] but the various factors impinging upon the overall transport process plus the possible number of analytes of physiologic relevance dictate the need for a more complex microfluidic model. Transient conditions also yield invaluable information for tracking blood glucose changes.

Biomarkers present in the skin originate predominantly in the bloodstream, for which the capillaries are densest within 2 plexuses: a superficial plexus located just beneath the dermal-epidermal junction, and a lower plexus residing in the hypodermis. Capillaries are also distributed throughout the dermal ISF, with local populations that encircle the hair follicle/SG appendages. For modeling blood-to-sweat transport, the appropriate transport mechanisms are used for each domain (Fig. 1).

Mass Transport Through Capillary Walls

Materials are transported through the capillary endothelial cells into ISF via diffusion and hindered convection. Modeling blood-to-tissue mass transport is based on the Ibrahim and Kasting analysis,[11] modified to reflect appropriate analyte ISF concentrations, yielding a clearance constant k_{de}. The study by Ibrahim et al.[11] has complete details. This clearance value is then used in ISF transport modeling to calculate a biomarker source term.

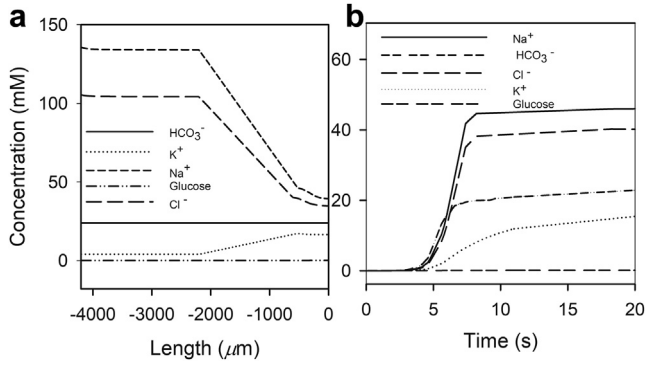

Figure 2. (a) Concentration profile of select biomarkers along the sweat duct length, beginning at the bottom of the sweat gland and ending at the skin surface (z = 0 μm). (b) Concentration-time profile of emergent sweat, using t = 0 to indicate the beginning of sweat stimulation at the base of the gland. Modeling used a sweat rate of 5 nL/min/gland.

Mass Transport Through Well-Stirred Dermal ISF

A uniform capillary distribution assumption renders the ISF well stirred (uniform concentration). This simplifies the modeling process because the entire domain can be treated on a compartmental basis, resulting in a computational savings. Ordinary differential equations account for both any cellular uptake (metabolism) and analyte source terms specific to the skin layers of viable epidermis (VE) and dermis (DE):

$$V_k \frac{\partial C_{i\,k}}{\partial t} = J_{source\ i} - k_{uptake\ i\ k}\, V_k \qquad (1)$$

where subscript k denotes the ISF section corresponding to specific sweat duct domains (i.e., VE, upper DE, lower DE), V_k is the volume associated with layer k and the molar biomarker i source term, $J_{source\ i}$ (mol/s), is due to either the passive transport from the DE to VE layers because the latter lacks a blood supply (Eq. 2a)

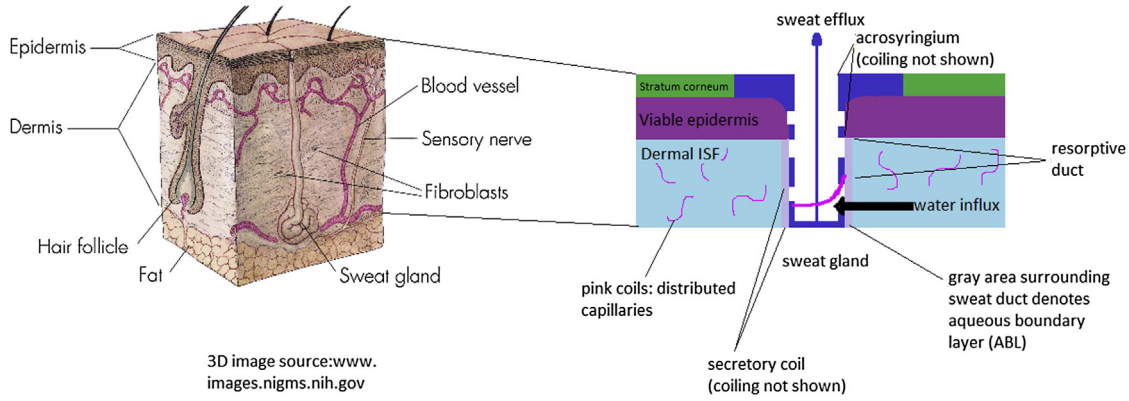

Figure 1. Assumed modeling geometry for sweat duct (right) with surrounding skin layers stratum corneum (SC), viable epidermis (VE), and dermal interstitial fluid (ISF), as shown in comparison to a realistic skin diagram. The gray section surrounding the gland denotes ISF devoid of capillaries, forming an aqueous boundary layer (ABL). Pink curves represent uniformly distributed ISF capillaries plus capillaries encircling the sweat duct base. Modeling was conducted on an axisymmetric basis around the duct centerline; in the modeling, the vertical length of duct is denoted by the *z*-axis (not shown). Transport phenomena and equations for each section are discussed in the main text and are biomarker dependent. Drawing not to scale.

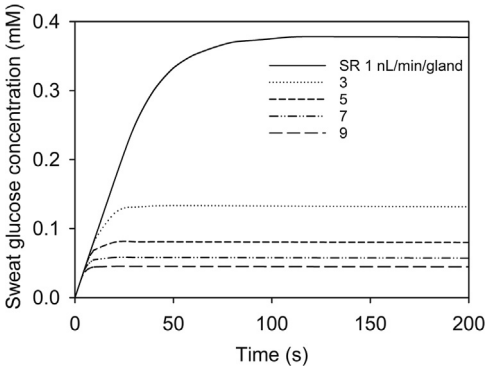

Figure 3. Glucose efflux concentration profiles as a function of sweat rate (SR), in nL/min/gland, and time (with t = 0 indicative of sweat stimulation in the base of the sweat gland) using a constant blood glucose level of 5mM.

$$J_{source\ i} = P_i S(C_{i\ DE} - C_{i\ VE}) \tag{2a}$$

$$J_{source\ i} = k_{de\ i} S(C_{i\ p} - C_{i\ ISF}) V_p \tag{2b}$$

or influx from the blood (DE layer, Eq. 2b) represented by the uniform capillary removal rate of analytes equal to the clearance constant previously determined, $k_{de\ i}$(1/s), times the local concentration gradient (i.e., plasma concentration minus ISF concentration). In the VE source term, P_i (cm/s) is biomarker permeability and S (cm^2) is transport area. For cases of negligible interstitial biomarker concentration, the plasma concentration in the DE source term serves as the driving force. In addition, biomarkers susceptible to fluctuating blood levels due to diet, stress, inflammation, environmental assaults, or exercise are handled through the clearance term.

For biomarkers that undergo metabolic uptake, for example glucose, the last term in Equation 1 accounts for biomarker consumption in each skin layer *k* via Michaelis-Menten kinetics:

$$k_{uptake\ i\ k} = \frac{V_{\max} C_{\ i}(t)}{K_m + C_{\ i}(t)} \tag{3}$$

where $k_{\text{uptake i}}$ is the biomarker uptake rate (mol/m^3s), $V_{\max}$ (mol/L s) the maximum uptake rate, K_m (mol/L) the analyte affinity constant, and C_i (*t*) (mol/L) the biomarker concentration in that domain. Table 1 lists the parameter values used for modeling glucose.

ISF initial conditions are contingent upon the biomarker of interest. Electrolyte concentrations (specifically Na^+, Cl^-, K^+ and HCO_3^-) are maintained at nearly isotonic levels with blood concentrations (Table 2). Conversely, other biomarkers are generally at negligible levels in the ISF, such as ethanol, present at baseline values corresponding to somewhat steady-state conditions, for example, glucose, or variable throughout the day, for example, cortisol.

It should be noted that the sweat values are representative; for example, K^+ concentrations in sweat are subject to interindividual variability and environmental variability.

The calculated domain concentrations dictate the boundary condition between the ISF and the aqueous boundary layer (ABL) domains encircling the sweat duct in the ABL transport equations, as described in the next section.

Table 1
Michaelis-Menten Parameters for Skin Glucose Uptake

Domain	$V \times 10^6$ (mM)	$K_m \times 10^3$ (mM)	Source
VE	8.4	0.5	14, 15
DE	47	6	13, 15
Hypo DE	44	5	12, 15

Table 2
Typical Ionic Concentrations (mM) of Select Electrolytes in Blood, ISF, Precursor, and Final Sweat

Electrolyte	Blood Plasma[21]	ISF[21]	Precursor Sweat[a]	Final Sweat[b]
Na^+	142	139	139	~48
Cl^-	108	108	108	~45
K^+	4	4	4-5	~14
HCO_3^-,	24	28	~28[c]	~3[d]

[a] Base of sweat gland.
[b] Sonner et al.[9]; Emergent on skin surface.
[c] Bovell.[22]
[d] Harvey et al.[23]

Mass Transport Through ABL ISF

Because local capillary populations supplying the SGs lie a discrete distance from the surface, the ISF portion adjacent to the SG is treated as an unperfused ABL. Transient 2-dimensional biomarker transport through the ABL sections is modeled on a diffusive basis only:

$$\frac{\partial C_{i\ k}}{\partial t} = D_{i\ k} \frac{\partial C^2_{i\ k}}{\partial z^2} \tag{4}$$

Here C_{ik} and D_{ik} are the analyte *i* concentration (mol/L) and diffusivity (cm^2/s) in domain *k* (*k* = VE, DE upper and lower), and *z* denotes transverse distance coordinate (cm), that is, depth below the surface opening, z = 0.

ABL ISF Boundary and Initial Conditions

As boundary conditions differ depending on the SG section in contact with the ABL ISF area, the ABL ISF domain is modeled in 3 compartments—upper layer pertaining to the epidermal region adjacent to the acrosyringium, middle layer corresponding to the resorption ductal region, and lower layer in contact with the secretory coil—using the previously determined analyte concentration boundary conditions and perfused ISF initial conditions. The mechanisms for electrolyte transport into each ductal region are discussed in the next 3 sections.

Secretory Portion ISF Boundary Conditions

Transport along the axial length of the secretory coil circumference into the SG lumen occurs by 2 means—active Cl^- ion[24] transport (under direct basolateral Na-K-Cl [NKCC] cotransporter control), which then dictates the corresponding Na^+ flux, or passive transport for other electrolytes and uncharged biomarkers. Thus, Na^+ and Cl^- fluxes are modeled to reflect the physiological functioning of the NKCC cotransporter based on a steady-state flux approximation,[25,26] mathematically described by

$$J_{NKCC} = \rho_{NKCC}\ \upsilon_{NKCC} \tag{5}$$

where ρ_{NKCC} is the cotransporter density within the membrane and υ_{NKCC}, the transporter turnover rate, is given by:

$$\upsilon_{NKCC} = \frac{k_f^{full} k_f^{empty} \gamma^4 Cl_s^2 K_s Na_{\ s} - k_b^{full} k_b^{empty} \gamma^4 Cl_i^2 K_i Na_{\ i}}{\sum_{n=1}^{16} Z^n_{NKCC}} \tag{6}$$

In Eq. 6, the pump variables represent the following: *k*, rate constant values for forward f and backward b reactions; γ, activity coefficient; and Cl, Na, K, electrolyte concentrations (here *i*

denotes intracellular [luminal] and *s* serosal [extracellular]); more detailed cotransporter information can be found in the study by Benjamin and Johnson.[26] HCO_3^- and K^+ fluxes are modeled through continuity and partitioning conditions at the ISF/SG interface because these are transported into the lumen at rates sufficient to maintain concentration levels in equilibrium with ISF concentrations:

$$K_{SG/ISF} = \frac{C_{SG}}{C_{ISF}} \tag{7a}$$

$$D_{i\ ISF}\frac{\partial C_{i\ ISF}}{\partial z} = D_{i\ SG}\frac{\partial C_{i\ SG}}{\partial z} \tag{7b}$$

The end result is precursor sweat generation that is essentially isotonic with ISF insofar as Na^+, Cl^-, K^+, and HCO_3^- concentrations. Passive diffusion for other biomarkers, such as glucose, is also modeled for this SG section.

Water flux across the membrane $J_{w\ TM}$ (m^3/s) (equal to the ABL ISF water efflux) is modeled as a laminar flow rate physiologically controlled by the osmotic gradient established by (mainly) Cl^- and Na^+ luminal influx via[27]

$$J_w^{TM} = L_p^{TM}\ \nu_w\ SA\left(\Delta C_i^{TM}\right) \tag{8}$$

where $L_{p\ TM}$ is the transmembrane (TM) hydraulic water conductivity (μm/s), ν_w the partial molar volume of water (m^3/mol), SA the surface area impacting the water flux (m^2), and the TM concentration gradient of biomarker i, $\Delta\ C_i^{TM}$, is in mOsm/L. Typical sweat rates range from 1-5 nL/min/gland, with 0.5 nL/min/gland assumed for passive sweating and enhanced sweating close to 9 nL/min/gland.

Resorptive Duct ISF Boundary Conditions

The resorptive fluxes of Na^+ and Cl^- of the lumen[24] via the epithelial sodium channel and cystic fibrosis transmembrane regulator transporters, respectively, are modeled to reflect the physiologic functioning of the epithelial basolateral NaK[25,28] pump based on a steady-state flux approximation mathematically described by

$$J_{NaK} = \rho_{NaK}\ \upsilon_{NaK} \tag{9}$$

where $\rho_{\ NaK}$ is the membrane pump density and υ_{NaK}, the pump turnover rate, is given by

$$\upsilon_{NaK} = \frac{\alpha_1^+\ \alpha_2^+\ \alpha_3^+\ \alpha_4^+ - \alpha_1^-\ \alpha_2^-\ \alpha_3^-\ \alpha_4^-}{\Sigma} \tag{10}$$

Additional details about the forward (+) and backward (−) apparent reaction rates, $\alpha_{1,2,3,4}^{\pm}$, which comprise forward and backward rate and equilibrium constants of the individual reaction steps, and other pump details can be found in the study by Smith and Crampin.[28] The actions of these facilitators renders the final sweat hypotonic compared to precursor levels.

Supplemental resorptive fluxes include additional lumen-to-ISF fluxes for Na^+ and Cl^- (due to the presence of redundant ion channels), as well as ISF-to-lumen boundary fluxes for K^+, H^+, HCO_3^-, the latter evidenced by the lower pH reported in final sweat, the increase in potassium in final sweat compared to blood and ISF (Table 2), and in predicting electrolyte concentrations in final sweat for cystic fibrosis conditions for a given sweat rate.[9]

Mass Transport Through Sweat Gland

Convective and diffusive transport occurs within the ductal secretory and resorptive regions for uncharged biomarkers. For electrolytes, the driving force includes electrodiffusion and electrostatic interactions with the charged pores, with transient axial biomarker transport modeled via:

$$\frac{\partial C_{i\ m}}{\partial t} = D_{i\ m}\frac{\partial^2 C_{i\ m}^2}{\partial z^2} + u\frac{\partial C_{i\ m}}{\partial z} + z_i\frac{D_{i\ m}\ F}{RT}\left(\frac{\partial}{\partial z}\left(C_{i\ m}\frac{\partial \psi}{\partial z}\right)\right) \tag{11}$$

where z_i is the biomarker charge, ψ electrical potential (V), u solvent velocity (m/s), and m represents the 3 SG sections (secretory coil, resorptive duct, and acrosyringium). For nonelectrolytes, the last term in Equation 11 drops out.

SG Initial and Boundary Conditions

Biomarker concentrations are initially assumed to be zero throughout SG sections. Boundary flux conditions for the secretory and resorptive portions of the SG correspond to the bidirectional fluxes for Na^+, Cl^-, and K^+ described previously in the ABL ISF boundary condition sections; passive ISF-to-lumen diffusion of uncharged biomarkers is also modeled. Because the acrosyringium is intraepidermally located, only passive diffusion of uncharged biomarkers into the SG will be modeled for the acrosyringium portion that is located within the VE.

Applied Electrical Field

The impact from applied electrical fields, subject to time of treatment, affects the biomarker ductal permeability via epithelial cell wall pore creation. Applied fields can also serve as a mechanism for SG secretion and modulation (i.e., sweat stimulation [via iontophoretic cholinergic administration], sweat augmentation [via reverse iontophoresis], increased biomarker paracellular permeability, which is especially important under low sweat rate conditions where the analyte detection level limits are already low). Thus, electrical techniques not only affect ductal lining integrity but also impact the sweat rate, and ultimately sweat concentrations. The model presently handles the electrically enhanced data in a macroscopic manner via a global permeability coefficient termed P_{wall}. This approach is advantageous in that a passive permeability coefficient can be devolved from data under similar conditions. Notably, this coefficient can also be segregated into the various electrical field components, given sufficient suitable data; this work is the subject of future studies.

Temporal Conditions of Blood Glucose and Sweat Rate

Blood glucose and sweat rate can display temporal effects. For blood glucose changes, glucose administration (ingestion or intravenous) raises blood levels, which impacts the skin insulin response (i.e., glucose uptake). Similarly, direct insulin administration causes the increased uptake, lowering blood glucose levels. Meal ingestion, especially of high glycemic foods, plays a similar role to glucose administration. Sweat rates, which vary between thermal or chemical stimuli, exhibit a sharp uptick after exposures followed by a gradual decay upon stimuli cessation. Differing sweat electrolytes levels based on the sweat rate can most likely be attributed to the limited capability of pump activity in the resorptive duct section (i.e., pump functionality reaches a maximal level). In the model, both glucose and sweat rate temporal changes are handled as tabulated input parameters, while the sweat rate variability is tied to pump turnover rate. To allow for an estimate of the

pump/cotransporter turnover rate for each sweat level, sweat electrolyte concentrations were modeled over a range of discrete sweat rates.

Computational Details

Time-dependent simulations were performed using COMSOL® Multiphysics finite element analysis platform (Burlington, MA). Two-dimensional axisymmetric transport was modeled within domains comprised of the ABL ISF and SG sections. Initial and boundary conditions are biomarker-dependent. COMSOL automatically implements the best solver, but a default override is available. Simulations used the PARDISO direct default solver with absolute and relative tolerances of 0.001 and 0.01, respectively.

Results and Discussion

This work represents, for the first time, glucose transport modeling from systemic circulation and into sweat.

Electrolyte Levels

The foundational dynamic flow model initially developed for blood/ISF-to-sweat electrolyte transport entailed modeling the sweating cascade/resorption processes and ensuing osmotically driven water influx into the duct. Based on a nominal sweat rate of 5 nL/min/gland, the modeling of select key electrolytes (Na^+, Cl^-, K^+, and HCO_3^-, which play primary roles in the sweating process yet have stable interstitial concentrations) yielded electrolyte transport through (Fig. 2a) and emerging from (Fig. 2b) the SG. Due to the homeostatic nature of the body regarding these electrolytes in blood and ISF, the main kinetics involved are those associated with sweat duct transport; thus, through the resorptive and passive ductal transport functions, only affected electrolytes display altered levels in Figure 2. Modeling reproduces the typical values of electrolytes at the base of the SG and sweat efflux based on steady-state plasma, ISF, precursor sweat, and final sweat values (Table 2).

While varying sweat rates dictate sweat Na^+ and Cl^- efflux values, glucose transport is affected by sweat rate changes for multiple reasons.

Glucose Levels

Glucose sensing via sweat monitoring uses different methods for fluid generation: thermal sweating,[29] which relies on hypothalamus signaling, and chemically stimulated sweating, specifically iontophoretic administration of Ca^{2+} agonists, for example acetylcholine, carbachol, methylcholine. Thermal sweating is more variable[29] compared to chemically induced sweating, but both dissipate over time and acclimatize after multiple exposures. The model accommodates for physiologic sweating (initiation methods and sweat dissipation) via modulation of sweat rates.

Sweat rate variability is particularly important for glucose because it impacts the corresponding sweat efflux analyte levels. Sweat glucose at a sweat rate of 9 nL/min/gland (profuse sweating) is diluted over that at 1 nL/min/gland (slightly above passive/intrinsic sweating), as shown in the sensitivity analysis of the effect of the sweat rate on sweat glucose concentrations (Fig. 3).

Calibration—Glucose

Many studies measure steady-state ratios between blood and various bodily fluids (ISF, saliva, tears, sweat). More pertinent from a glucose monitoring perspective are the glucose profiles within these domains over time. In contrast to key electrolyte transport, sweat glucose levels reflect metabolic skin uptake mechanisms that are predicated upon temporal physiologic blood concentrations, for example, diabetic glucose swings, nondiabetic fasting. The temporal skin glucose levels in turn impact sweat efflux levels.

Sweat glucose levels were modeled using literature and experimental data under different conditions of blood glucose and sweat rate for both healthy and diabetic subjects (Fig. 4). Under passive sweating, healthy subjects in the Lee et al.[30] investigation displayed blood glucose peaks and troughs corresponding to alternating periods of meal ingestion followed by fasting interludes (Fig. 4a). The sweat rate in that case was estimated at 0.5 nL/min/gland. Similar spikes and dips were observed in sweat glucose levels, albeit at slightly lower concentrations; simulated sweat data closely match the experimental data. Because sweat data were gathered at the same discrete time points as the blood draws, glucose lag time is not obvious. However, lag time can be estimated from the difference between blood and simulated sweat peaks (~5 min), which is within the range reported in the literature.[3,4,33-35] With glucose ingestion and infusion (standard glucose tolerance test bolus of 100g glucose dissolved in 10 oz. water and 25 g glucose in 25 mL water intravenously), healthy subjects in the Boysen et al.[31] study incurred much larger blood glucose swings (Fig. 4b). Sweat initiation/maintenance for these subjects resulted from thermal stimuli (sauna exposure), whereby a stable 50°C air temperature corresponded to ~8 nL/min/gland sweat rate. Despite the higher blood glucose levels, sweat glucose dilution is evident compared to the passive sweating data. Simulated sweat data, in agreement with experimental data, showed a similar time lag after glucose intravenous infusion (1500 s blood glucose peak revealed as ~1750-2000 s sweat peak). Both experimental and simulated sweat data in that study trend with the blood glucose changes, except at the end when blood glucose levels off and the sweat levels continue to

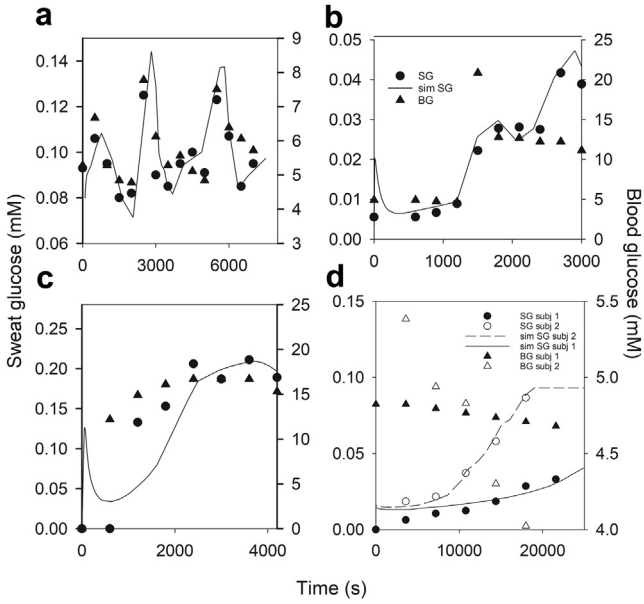

Figure 4. Simulated sweat data (lines) compared to experimental data (symbols) from (a) Lee et al.,[30] variable blood glucose (via meals), stable low sweat rate, and healthy subjects; (b) Boysen et al.,[31] variable blood glucose (via glucose ingestion/intravenous infusion), stable, high (8 nL/min/gland) sweat rate, and healthy subjects; (c) Moyer et al.,[32] variable blood glucose (via glucose/insulin administration), estimated variable sweat rate, and diabetic subjects; (d) present study, fasting glucose conditions, measured carbachol-initiated sweat rates (baseline rate to 5 nL/min/gland, followed by decline), and healthy subjects. Symbols: sweat glucose (SG): circles; blood glucose (BG): triangles. Here, time is measured relative to blood glucose measurements (t = 0 at initial blood glucose measurement).

increase. A partial explanation for the observed discrepancy might lie with the estimation of sweat rate decline, especially because lower sweat rates would impact sweat glucose levels greatly (Fig. 3:~9-fold sweat glucose dilution corresponds to a 9-fold sweat rate increase). The objective of the Moyer et al.[32] study (Fig. 4c) was to show a correlation between sweat and blood glucose; to achieve sizable blood glucose swings, diabetic patients were administered glucose (a solution containing 75 g glucose if initial BG was normal or low) or insulin (for high initial BG levels at a dose instructed by a physician). Furthermore, the sweat rate range, iontophoretically initiated via pilocarpine administration, was estimated, not measured. For modeling, a passive a sweat rate of 0.5 nL/min/gland was assumed before iontophoresis, followed by a 5 nL/min/gland peak sweat rate immediately after sweat initiation, with a gradual return to the passive sweat rate. As with the Boysen data, experimental and simulated sweat data in the Moyer study are well correlated, except during initial increasing sweat rates. The assumption of a dramatic sweat rate increase just after iontophoretic stimulation may explain the lower simulated result compared to experimental data. A different sweat rate profile, although it might improve the data agreement, cannot be defended over the assumed ramping rate.

In the present study, experimental electrically enhanced sweat glucose data were obtained from 2 healthy subjects under fasting conditions, concurrently with sweat rate measurements and blood glucose draws (Fig. 4d). Counter to diminishing blood glucose levels, experimental glucose concentrations in sweat rose over time in response to the decay in the sweat rate after iontophoresis ceased. The different sweat glucose profiles highlight the intersubject variability of *in vivo* sweating due to gender, age, acclimatization, and other factors.[36] Simulated sweat data were in agreement with experimental values. The small drop in blood glucose levels, compounded by inter- and intra-subject sweating variability, precludes an accurate estimation of lag time from the data. The average sweat/blood glucose levels in Figure 4 ranged from 0.001 to 0.02 for both experimental and simulated ratios, varying according to the sweat rate.

The intersubject variability displayed in Figure 4d is one of several known factors that impacts sweat analyses. For example, physical fitness impacts sweat production, as does repeated heat exposures, age, gender, and bodily site. Studies conducted in our laboratory for sweat stimulation feasibility have shown significant age and gender differences, in particular.[36] Despite control of many factors in this study (time of day for conducting experiments, stimulation of sweat in a controlled manner, fasting subjects, precise bodily location for sweat procurement, etc.), age and gender differences were not controlled. Reasons for this include the small number of overall subjects and unequal gender distribution; hence, no attempt was made to investigate or model gender and age differences as distinct factors. Instead, the differences are modeled herein through blood concentration, sweat rate, uptake kinetics, and epithelial glucose permeability coefficient. The latter is particularly important as it facilely lends itself to the application of electrical field applications, which directly impact ductal epithelial permeabilities.

Modeling simulated sweat glucose data to experimental sweat glucose data highlighted the importance of certain parameters in sweat biomarker concentrations. Specifically, 4 parameters (Fig. 5)—skin layer metabolic uptake, dermal clearance constant, epithelial glucose permeability, and sweat rate—played a significant role in the fitting process, although in differing capacities. For example, the sweat rate is critical and was measured experimentally. In addition, dermal clearance was calculated from measured blood glucose concentrations using calculated dermal diffusivities of solutes. Thus, only 2 parameters, metabolic uptake rates and epithelial glucose permeability, were fitted to match the simulated and experimental data, given the constraint of the other parameters. The interplay between skin metabolism of glucose and sweat glucose transport is significant, mainly due to the overwhelming influence of skin concentrations impacted by glucose skin kinetics compared to the passive sweat duct epithelial transport of glucose and the rapid convective transport of glucose through the duct. An alternative approach for future studies would be experimental determination of the metabolic skin rate variables, leaving only a fitted epithelial permeability coefficient. Parametric sweeps for sensitivity studies would also be beneficial in a follow-up study.

Herein, sweat duct permeability to glucose has been modeled in terms of a global permeability coefficient, *P*, without any specification of the transport mechanism across the epithelial cell layers comprising the sweat duct wall. Some glucose may enter the duct naturally with the osmotic flow of water in the secretory coil. This transport is augmented by carbachol iontophoresis (Fig. 4d). Possible mechanisms for this enhancement include electroporation of the epithelial cell membranes as proposed by Chizmadzhev et al.[37] and/or electroosmosis through tight junctions.[18] Both phenomenon would be most likely to occur in the resorptive duct rather than the secretory coil due to the higher electric field in the former region.[37] The extent to which the permeability is increased by such treatments and the duration of this effect are of

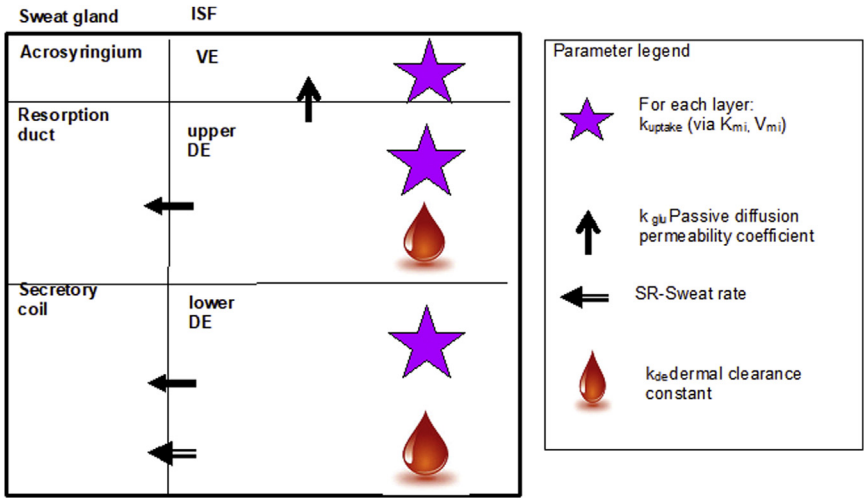

Figure 5. Critical parameters in the determination of the concentration and transport rate of glucose from the blood to sweat include k_{uptake}, P, SR, and k_{de}.

considerable interest in understanding the relationship between sweat and blood glucose levels. This question forms the basis for further study in our laboratory.

Conclusions

The computational model quantitatively describes the various processes of sweat analyte transport originating from systemic distribution, including sweat initiation and metabolic skin uptake dynamics. Key electrolytes were modeled within the sweating cascade as well as glucose, important from a diagnostic health perspective. The glucose model, calibrated under a variety of experimental conditions including electrical enhancement, revealed a 10 min blood-to-sweat lag time and a sweat/blood glucose level ranging from 0.001 to 0.02, depending on the sweat rate.

Acknowledgments

This work was supported by NSF Award #1608275. The authors are grateful to Dr. Kevin Li for providing the COMSOL computational software license.

References

1. American Diabetes Association. Available at: http://www.diabetes.org/diabetes-statistics. Accessed November 1, 2017.
2. Klonoff DC. Continuous glucose monitoring—roadmap for 21st century diabetes therapy. *Diabetes Care*. 2005;28:1231-1239.
3. Tierney M, Tamada JA, Potts R, Jovanovic L, Garg S. Clinical evaluation of the GlucoWatch biographer: a continual, non-invasive glucose monitor for patients with diabetes. *Biosens Bioelectron*. 2001;16:621-629.
4. Rao G, Guy R, Glikfeld P, et al. Reverse iontophoresis: noninvasive glucose monitoring *in vivo* in humans. *Pharm Res*. 1995;12:1869-1873.
5. Stout P, Peled N, Erickson B, Hilgers M, Racchini J, Hoegh T. Comparison of glucose levels in dermal interstitial fluid and fnger capillaries. *Diabetes Technol Ther*. 2001;3:81-90.
6. Vashist SK. Non-invasive glucose monitoring technology in diabetes management: a review. *Anal Chim Acta*. 2012;750:16-27.
7. National Institute of Diabetes and Digestive and Kidney Diseases. Continuous glucose monitoring. Available at: https://www.niddk.nih.gov/health-information/diabetes/managing-diabetes/continuous-glucose-monitoring. Accessed November 1, 2017.
8. Bandodkar AJ, Wang J. Non-invasive wearable electrochemical sensors: a review. *Trends Biotechnol*. 2014;32:363-371.
9. Sonner Z, Wilder E, Heikenfeld J, et al. The microfluidics of the eccrine sweat gland, including biomarker partitioning, transport and biosensing implications. *Biomicrofluidics*. 2015;9:031301.
10. Stern R. The diagnosis of cystic fibrosis. *N Engl J Med*. 1997;336:487-491.
11. Ibrahim R, Nitsche JM, Kasting GB. Dermal clearance model for epidermal bioavailability calculations. *J Pharm Sci*. 2012;101:2094-2108.
12. Kozka IJ, Clark AE, Reckless JPD, Cushman SW, Gould GW, Holman GD. The effect of insulin on the level and activity of the GLUT4 present in human adipose cells. *Diabetologia*. 1995;38:661-666.
13. Longo N, Griffin LD, Shuster RC, Langley S, Elsas LJ. Increased glucose transport in human fibroblasts with a heritable defect in insulin binding. *Metabolism*. 1989;38:690-697.
14. Spravchikov N, Sizyakov G, Gartsbein M, Accili D, Tennebaum T, Wertheimer E. Glucose effects on skin keratinocytes. Implications for diabetes skin complications. *Diabetes*. 2001;50:1627-1635.
15. Groenendaal W, Schmidt KA, von Basum G, van Riel NA, Hilbers PA. Modeling glucose and water dynamics in human skin. *Diabetes Technol Ther*. 2008;10:283-293.
16. Dancik Y, Miller M, Jaworska J, Kasting GB. Design and performance of a spreadsheet-based model for estimating bioavailability of chemicals from dermal exposures. *Adv Drug Deliv Rev*. 2013;65:221-236.
17. Kasting GB, Nitsche JM. Mathematical models of skin permeability: microscopic transport models and their predictions. In: Querleux B, ed. *Computational Biophysics of the Skin*. Singapore: Pan Stanford; 2014:187-216.
18. Jajack A, Brothers M, Kasting G, Heikenfeld J. Enhancing glucose flux into sweat by increasing paracellular permeability of the sweat gland. *PLoS One*. 2018;13(7):e0200009.
19. Sonner Z, Wilder E, Gaillard T, Kasting GB, Heikenfeld J. Integrated sudomotor axon reflex sweat stimulation for continuous seat analyte analysis with individuals at rest. *Lab Chip*. 2017;17:2531-2684.
20. Simmers P, Li S, Kasting G, Heikenfeld J. Prolonged and localized sweat stimulation by iontophoretic delivery of the slowly-metabolized cholinergic agent carbachol. *J Dermatol Sci*. 2018;89:40-51.
21. Friedman MH. *Principles and Models of Biological Transport*. 2nd ed. New York: Springer; 2008.
22. Bovell D. The human eccrine sweat gland: structure, function and disorders. *J Local Glob Health Sci*. 2015;5:1-16.
23. Harvey CJ, LeBouf RF, Stefaniak AB. Formulation and stability of a novel artificial human sweat under conditions of storage and use. *Toxicol In Vitro*. 2010;24:1790-1796.
24. Frizzell RA, Hanrahan JW. Physiology of epithelial chloride and fluid secretion. *Cold Spring Harb Perspect Med*. 2012;2:a009563.
25. O'Donoghue DL, Dua V, Moss GWJ, Vergani P. Increased apical Na^+ permeability in cystic fibrosis is supported by a quantitative model of epithelial ion transport. *J Physiol*. 2013;15:3681-3692.
26. Benjamin BA, Johnson EA. A quantitative description of the Na-K-2Cl cotransporter and its conformity to experimental data. *Am J Physiol*. 1997;273(Renal Physiol 42):F473-F482.
27. Latta R, Clausen C, Moore LC. A generalized method for the derivaion and numerical solution of epithelial transport models. *J Membr Biol*. 1984;82:67-82.
28. Smith NP, Crampin EJ. Development of models of active ion transport for whole-cell modelling: cardiac sodium-potassium pump as a case study. *Prog Biophys Mol Biol*. 2004;85:387-405.
29. Sato K, Feibleman C, Dobson RL. The electrolyte compostition of pharmacologically and thermally stimulated sweat: a comparative study. *J Invest Dermatol*. 1970;55:433-438.
30. Lee H, Choi TK, Lee YB, et al. A graphene-based electrochemical device with thermoresponsive microneedles for diabetes monitoring and therapy. *Nat Nanotechnol*. 2016;11:566-572.
31. Boysen TC, Yanagawa S, Sato F, Sato K. A modified anaerobic method of sweat collection. *J Appl Physiol Respir Environ Exerc Physiol*. 1984;56:1302-1307.
32. Moyer J, Wilson D, Finkelshtein I, Wong B, Potts RO. Correlation between sweat glucose and blood glucose in subjects with diabetes. *Diabetes Technol Ther*. 2012;14:398-402.
33. Steil GM, Rebrin K, Hariri F, et al. Interstitial fluid glucose dynamics during insulin-induced hypoglycaemia. *Diabetologia*. 2005;48:1833-1840.
34. Kulcu E, Tamada JA, Reach G, Pots RO, Lesho MJ. Physiological differences between interstitial glucose and blood glucose measured in human subjects. *Diabetes Care*. 2003;26:2405-2409.
35. Tamada JA, Comyns K. Effect of formulation factors on electroosmotic glucose transport through human skin *in vivo*. *J Pharm Sci*. 2005;94:1839-1849.
36. Wilder ECS. *Human Subjects Testing of Sweat Stimulation Technologies*. Cincinnati, OH: Winkle College of Pharmacy, University of Cincinnati; 2016.
37. Chizmadzhev YA, Indenbom AV, Kuzmin PI, Galichenko SV, Weaver JC, Potts RO. Electrical properties of skin at moderate voltages: contribution of appendageal macropores. *Biophys J*. 1998;74:843-856.